Terahertz wedge plasmon polaritons

A. I. Fernández-Domínguez,[1,*] Esteban Moreno,[1] L. Martín-Moreno,[2] and F. J. García-Vidal[1]

[1]*Departamento de Física Teórica de la Materia Condensada, Universidad Autónoma de Madrid, E-28049 Madrid, Spain*

[2]*Departamento de Física de la Materia Condensada and Instituto de Ciencia de Materiales de Aragón (ICMA), Centro Superior de Investigaciones Científicas (CSIC)–Universidad de Zaragoza, E-50009 Zaragoza, Spain*

**Corresponding author: anisaac.fernandez@uam.es*

Received February 5, 2009; revised April 16, 2009; accepted May 4, 2009; posted June 3, 2009 (Doc. ID 107179); published June 29, 2009

We propose a metamaterial approach to route terahertz waves that features subwavelength confinement in the transverse plane. The guiding mechanism is based on geometrically induced electromagnetic modes sustained by corrugated metallic wedges, whose characteristics resemble those of wedge plasmon polaritons at telecom and optical frequencies. Additionally, frequency selective focusing and slowing down of terahertz radiation based on the proposed wedge waveguides are presented. © 2009 Optical Society of America

OCIS codes: 240.6680, 300.6495, 130.2790.

Terahertz (THz) radiation bears great potential in a broad range of technological areas such as medical diagnostics, sensing, product quality control, or security imaging [1]. The emergence of compact THz circuits requires the design of functional elements of sizes comparable to THz wavelengths (between tens of microns to several millimeters). In the optical regime, surface plasmon polaritons (SPPs) have demonstrated excellent capabilities for achieving transport and subwavelength confinement of electromagnetic (EM) energy. However, although SPPs at THz frequencies present longer propagation lengths [2,3], their extended size makes them not suitable for routing applications. Recently, the concept of geometrically induced (or spoof) SPPs [4,5] has opened the way for the transfer of SPP characteristics in the visible to lower frequencies. The spoof SPP concept was first realized experimentally on planar geometries [6,7], but lately it has been also extended to wire geometries [8,9], where high transverse confinement of THz waves has been demonstrated.

In this Letter, we present a planar scheme for guiding THz waves displaying subwavelength transverse (lateral and vertical) confinement and low attenuation. The design consists of a metallic wedge milled with a periodic array of grooves. We demonstrate that such geometry sustains spoof SPPs, which resemble wedge plasmon polaritons (WPPs) [10] in the visible range. The upper panel of Fig. 1 shows the proposed structure. The geometric parameters defining the wedge are the height, h, and the angle, θ. The grooves milled on the wedge have depth t and width a, and the period of the corrugation is d. To make our design work at THz frequencies, we choose the period $d=200$ μm. Additionally, we fix $a=100$ μm and $h=1$ mm. We model the metal as a perfect electric conductor (PEC), which is an excellent approximation for real metals in the THz regime.

The lower panel of Fig. 1 renders the two lowest bands of the spoof WPPs traveling along wedges with $\theta=20°$. The wedges are textured with grooves of three different depths (50, 100, and 150 μm). Dispersion bands are lowered as the groove depth, t, is increased. Owing to the finite height of the wedge, spoof WPP bands in Fig. 1 reach the light line, featuring a cutoff frequency as also observed in conventional WPPs [10]. Insets (a) and (b) depict the longitudinal component of the electric field at the band edge ($k=\pi/d$) for the two spoof WPP modes supported by the structure with $t=100$ μm (squares). The cross sections correspond to the deeper part of the corrugated wedge, where the EM fields are mostly localized (solid and dashed lines indicate the inner and outer wedge outlines). Inset (a), which renders the first spoof mode, displays only one maximum within the transverse plane. However, the electric field associated to the second WPP, shown in inset (b), presents two lobes of different sign along the vertical direction, vanishing in the horizontal plane between them. Note that both EM modes have even parity with respect to the vertical symmetry plane. Both dispersion relations and electric fields shown in

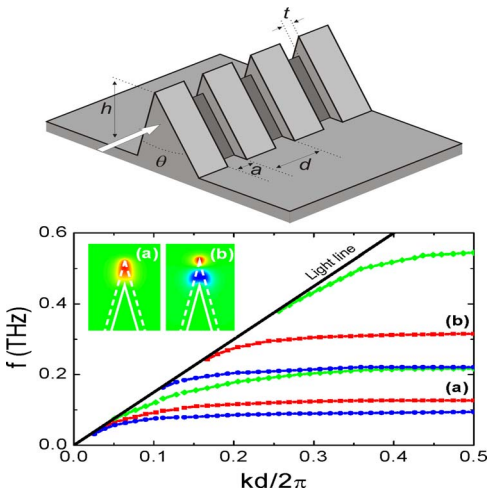

Fig. 1. (Color online) Upper panel, sketch of the proposed waveguiding scheme. White arrow indicates the direction of propagation. Lower panel, two lowest spoof WPP bands for wedges with three different depths, t: 150 μm (circles), 100 μm (squares), and 50 μm (diamonds). The rest of the geometric parameters are described in the text. Insets (a) and (b) show snapshots of the longitudinal component of the electric field at the edge of the two bands for the case $t=100$ μm.

Fig. 1 have been obtained from finite-difference time-domain (FDTD) calculations with an square mesh size of 5 μm.

Once we have demonstrated that periodically corrugated PEC wedges support spoof WPP modes whose dispersion relation can be controlled by the groove depth, we study the influence of the angle, θ, on the modal characteristics. In Fig. 2, the fundamental WPP bands for wedges of different θ are shown (for all structures, a and d remain as in Fig. 1, and $t=100$ μm). As θ increases, the bands shift to higher frequencies, tending to the limiting case of a flat ($\theta=180°$) groove array [5]. The insets of Fig. 2 render the electric field amplitude at the band edge for wedges with (a) $\theta=20°$ and (b) $\theta=60°$. In both cases, the half-wavelength ($\lambda/2$) is represented by vertical white bars. Following the convention used for WPPs at higher frequencies [10], the modal size (δ) is defined as the transverse separation between the locations where the electric field amplitude has fallen to one tenth of its maximum value. Thus, the modal size for the 20° wedge is $\delta=656$ μm$=0.28\lambda$, whereas for $\theta=60°$, it is equal to 806 μm$=0.78\lambda$. These results demonstrate the subwavelength transverse confinement featured by spoof WPPs, the more so for sharper angles.

The presented modes, being below the light line, are, by definition, nonradiative. Therefore, losses can arise only when considering absorption, which was not taken into account in our previous PEC modeling. To estimate the propagation length, $l=[2\ \mathrm{Im}(k)]^{-1}$, associated with absorption in real corrugated wedges operating at THz frequencies, finite integration technique (FIT) simulations are performed. We consider a corrugated aluminum wedge with $\theta=60°$ (the remaining geometric parameters being the same as in Fig. 2) and a length of 40 mm, corresponding to 200 periods. Aluminum permittivity is taken from [11]. The mode propagation length is obtained by fitting the exponential decay of the electric field amplitude along the wedge. To illustrate the dependence of l on the frequency, we choose three representative values indicated by dotted arrows in Fig. 2. Close to the light line, at 0.16 THz, we find $l=120$ mm$=64\lambda$. At larger frequencies the propagation length is reduced, with $l=43.2$ mm$=29\lambda$ at 0.20 THz. Finally, as we approach the flat part of the band, the propagation length decreases abruptly. Thus, at 0.27 THz, we obtain $l=1.56$ mm$=1.3\lambda$. Notice that, as in conventional plasmonics, there is a trade off between the transverse confinement and propagation length. It is also remarkable that the values obtained for l/λ are comparable to those obtained for WPPs in the telecom regime [10], where the physical origin of the field confinement is completely different. This correspondence of l/λ between conventional and spoof SPPs has been also observed in planar and wire geometries [12,13].

Figure 2 provides us a hint on how THz waves can be focused and slowed down with the aid of spoof WPPs. The lowering of the dispersion bands for decreasing θ suggests that the radiation of a given frequency propagating in a wedge, which is sharpened along its length [see inset of Fig. 3(a)], would be gradually concentrated within the transverse plane. Additionally, THz waves at frequencies above the band edge associated to a specific θ will never reach sections of the structure sharper than that angle, being slowed down as they approach it. To prevent backreflection and scattering of EM fields out of such structure, impedance mismatches along the wedge length can be minimized by performing the reduction in θ adiabatically. The inset of Fig. 3(a) shows a diagram of the design proposed: a 10-mm-long wedge with θ varying smoothly from 60° to 20° milled by 50 grooves disposed periodically with the same geomet-

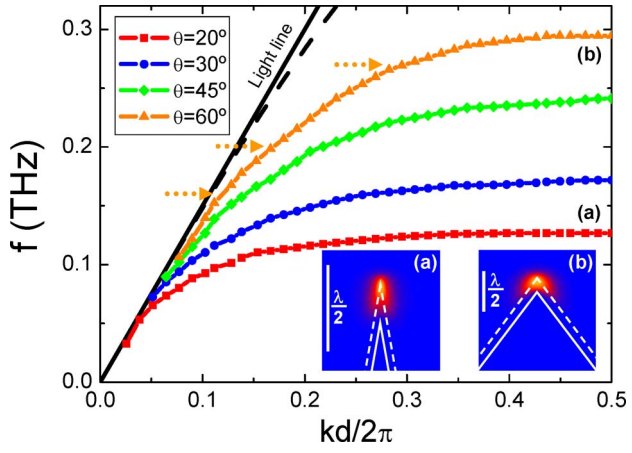

Fig. 2. (Color online) Dispersion relation of the fundamental spoof WPP traveling along corrugated wedges for different θ. Dashed black line shows the dispersion band corresponding to the flat ($\theta=180°$) case. The horizontal arrows indicate the frequencies for which the propagation length is estimated (see the text). Lower insets show the electric field amplitudes at the band edge for (a) $\theta=20°$ and (b) $\theta=60°$. In both insets, $\lambda/2$ is represented by white bars.

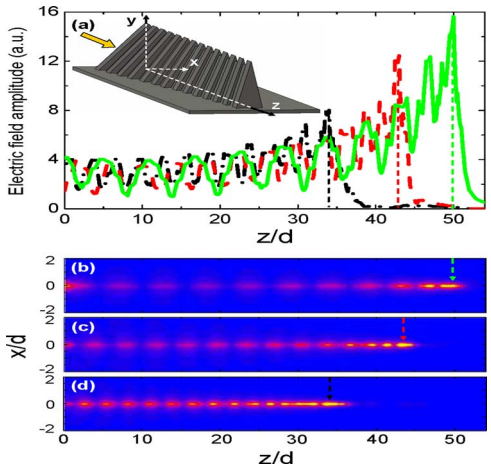

Fig. 3. (Color online) (a) Left inset, corrugated PEC wedge with θ varying smoothly along the z direction from 60° to 20°. Main panel, electric field amplitude versus z along the line located 100 μm above the structure apex. Three different frequencies are considered: 0.12 THz (solid curve), 0.16 THz (dashed curve), and 0.20 THz (dashed-dotted curve). Panels (b)–(d) depict the electric field amplitude within the xz plane located 100 μm above the apex for these three frequencies. Dashed arrows indicate the position of the maxima of amplitude shown in panel (a).

ric parameters as in Fig. 2. The guiding properties of the structure are studied by means of FIT simulations under PEC approximation. The wide end of the wedge is illuminated with a broadband pulse whose modal shape corresponds to that of spoof WPP modes supported by an infinitely long 60° wedge. Panel (a) in Fig. 3 renders the electric field amplitude, $|E|$, on a line parallel to the z axis and 100 μm above the wedge apex. $|E|$ is evaluated at three different frequencies within the spectral range spanned by the dispersion bands shown in Fig. 2. Waves at 0.12 THz (solid curve) propagate until the sharpest end of the wedge, giving rise to a maximum in the electric field amplitude located at that position. At higher frequencies, radiation is slowed down and stopped before reaching the wedge end. For $f=0.16$ THz (dashed curve), a peak in $|E|$ is developed at the 42nd groove, for which $\theta=26°$. At 0.20 THz (dashed-dotted curve) EM fields explore an even shorter section of the wedge, and $|E|$ presents a maximum at the 34th groove ($\theta=32°$). Note that these results are in excellent agreement with the FDTD dispersion bands of Fig. 2.

Panels (b)–(d) of Fig. 3 depict $|E|$ within the xy plane located 100 μm above the wedge apex for the three frequencies considered in panel (a). In these three contour plots, the reduction in the effective wavelength $[\lambda_{\mathrm{eff}}=2\pi\,\mathrm{Re}(k)^{-1}]$ experienced by the guided EM fields as they propagate along the structure can be observed, indicating that guided waves are not scattered out of the wedge as they travel in the z direction. On the contrary, while propagating along the structure, EM fields are gradually concentrated, giving rise to frequency selective focusing of THz waves.

In summary, we have shown that corrugated metallic wedges sustain geometrically induced EM guided modes. In the THz regime, these modes are particularly attractive owing to their low loss, excellent transverse confinement, and compatibility with planar technology. We have further demonstrated that by sharpening the wedge angle, lateral focusing of THz waves is achieved.

This work has been sponsored by the Spanish Ministry of Science under projects MAT2008-06609-C02 and CSD2007-046-NanoLight.es.

References

1. B. F. Ferguson and X.-C. Zhang, Nat. Mater. **1**, 26 (2002).
2. R. Mendis and D. Grischkowsky, Opt. Lett. **26**, 846 (2001).
3. K. Wang and D. M. Mittleman, Nature **432**, 376 (2004).
4. J. B. Pendry, L. Martín-Moreno, and F. J. García-Vidal, Science **305**, 847 (2004).
5. F. J. García-Vidal, L. Martín-Moreno, and J. B. Pendry, J. Opt. A **7**, S97 (2005).
6. A. P. Hibbins, B. R. Evans, and J. R. Sambles, Science **308**, 670 (2005).
7. C. R. Williams, S. R. Andrews, S. A. Maier, A. I. Fernández-Domínguez, L. Martín-Moreno, and F. J. García-Vidal, Nat. Photonics **2**, 175 (2008).
8. S. A. Maier, S. R. Andrews, L. Martín-Moreno, and F. J. García-Vidal, Phys. Rev. Lett. **97**, 176805 (2006).
9. A. I. Fernández-Domínguez, C. R. Williams, F. J. García-Vidal, L. Martín-Moreno, S. R. Andrews, and S. A. Maier, Appl. Phys. Lett. **93**, 141109 (2008).
10. E. Moreno, S. G. Rodrigo, S. I. Bozhevolnyi, L. Martín-Moreno, and F. J. García-Vidal, Phys. Rev. Lett. **100**, 023901 (2008).
11. M. A. Ordal, L. L. Long, R. J. Bell, S. E. Bell, R. R. Bell, R. W. Alexander, Jr., and C. A. Ward, Appl. Opt. **22**, 1099 (1983).
12. L. Shen, X. Chen, and T.-J. Yang, Opt. Express **16**, 3326 (2008).
13. L. Shen, X. Chen, Y. Zhong, and K. Agarwal, Phys. Rev. B **77**, 075408 (2008).